Behavior Research Methods, Instruments, & Computers
1998, 30 (1), 8-19

DATA ACQUISITION

Estimating the spatial Nyquist of the human EEG

RAMESH SRINIVASAN and DON M. TUCKER
University of Oregon, Eugene, Oregon
and Electrical Geodesics, Inc., Eugene, Oregon

and

MICHAEL MURIAS
University of California, Irvine, California
and Electrical Geodesics, Inc., Eugene, Oregon

Behavior Research Methods, Instruments, & Computers
1998, 30 (1), 8-19

DATA ACQUISITION

Estimating the spatial Nyquist of the human EEG

RAMESH SRINIVASAN and DON M. TUCKER
University of Oregon, Eugene, Oregon
and Electrical Geodesics, Inc., Eugene, Oregon

and

MICHAEL MURIAS
University of California, Irvine, California
and Electrical Geodesics, Inc., Eugene, Oregon

The discrete sampling of the brain's electrical field at the scalp surface with individual recording sensors is subject to the same sampling error as the discrete sampling of the time series at any one sensor with analog-to-digital conversion. Unlike temporal sampling, spatial sampling is intrinsically discrete, so that the post hoc application of analog anti-aliasing filters is not possible. However, the skull acts as a low-pass spatial filter of the brain's electrical field, attenuating the high spatial frequency information. Because of the skull's spatial filtering, a discrete sampling of the spatial field with a reasonable number of scalp electrodes is possible. In this paper, we provide theoretical and experimental evidence that adequately sampling the human electroencephalograph (EEG) across the full surface of the head requires a minimum of 128 sensors. Further studies with each of the major EEG and event-related potential phenomena are required in order to determine the spatial frequency of these phenomena and in order to determine whether additional increases in sensor density beyond 128 channels will improve the spatial resolution of the scalp EEG.

When the time series of an electroencephalogram (EEG) channel is sampled discretely, the Nyquist theorem specifies that the highest measurable frequency is half the sampling rate. For example, with a 250 sample/sec analog-to-digital conversion rate, the highest frequency that can be resolved is 125 Hz. In actuality, because of phase alignment, it is necessary to discretely sample (digitize) the signal at a rate at least 2.5 times the highest frequency component of the signal (Bendat & Piersol, 1986). Signal frequencies higher than the Nyquist frequency are not only poorly characterized; they *alias* or appear misleadingly as increased energy at lower frequencies. To avoid aliasing, it is necessary to eliminate the frequency components of the signal that are higher than the Nyquist frequency through analog filtering.

The electrical field of the brain generates a potential distribution that is continuous over the surface of the head. The discretization of this spatial EEG or averaged event-related potential (ERP) signal with scalp electrodes is also subject to the Nyquist theorem. If the spatial sampling is inadequate, high spatial frequencies will alias into low spatial frequencies, thereby distorting topographic maps, source localization, or other spatial analysis.

In this paper, we present simulations and data in order to estimate the number of spatial samples (sensors or electrodes) required to characterize human brain electrical activity across the full surface of the head with scalp EEG recordings. Mathematical simulations were conducted in order to estimate the influence of spatial filtering by the poorly conducting skull. For an empirical test, the visual ERP of a normal subject was sampled with 128 scalp sensors and then subsampled with 64, 32, and 19 sensors in order to determine the degree of undersampling and spatial aliasing that is associated with conventional recording procedures.

NYQUIST THEOREM FOR DISCRETE SAMPLING

The discrete sampling of continuous signals is a well-characterized problem in time series acquisition and analysis (Bendat & Piersol, 1986). The central concept is the Nyquist criterion:

$$f_{dig} > 2 * f_{max}, \quad (1)$$

where f_{dig} is the digitization or sampling rate and f_{max} is the highest frequency in the time series. For instance, if

Correspondence concerning this article should be addressed to D. M. Tucker, Electrical Geodesics, Inc., Riverfront Research Park, 1811 Garden Avenue, Suite 104, Eugene, OR 97403 (e-mail: dtucker@egi.com).

Note: Electrical Geodesics, Inc. sells 64-, 128-, and 256-channel EEG systems and thus has a commercial interest in promoting dense sensor array technology.—*Editor*

the signal is a sinusoid at 20 Hz (cycles/sec), a minimum sampling rate of 40 Hz (i.e., one sample every 0.025 sec) is required to record the signal digitally without aliasing. Aliasing appears as the misrepresentation of a high-frequency signal as a low-frequency signal because of undersampling, in violation of the Nyquist criterion. If a time series has been aliased because of undersampling, there is no valid method for removing or undoing the aliasing by digital signal processing methods.

Practical sampling requires a stiffer criterion, known as the engineer's Nyquist:

$$f_{dig} > 2.5 * f_{max}. \quad (2)$$

The engineer's Nyquist accounts for the possibility of phase-locking between the sinusoidal components of the signal and the sampling rate.

Consider the example shown in Figure 1A. This signal is the sum of three sinusoids of 6.5, 10, and 19 Hz. The signal is then sampled discretely at 100, 50, 20, and 10 Hz. As indicated by the power spectra in Figure 1B, the signal is well characterized at the sampling rates of 100 and 50 Hz, although it is instructive that some loss of the 19-Hz signal component is apparent even at 50 Hz. At the sampling frequency of 20 Hz, the signal is visibly distorted in the waveform plot, and the power spectrum shows the aliasing of the 19-Hz component to a low-frequency peak at ~2 Hz. Further reducing the sampling rate to 10-Hz produces a visibly distorted waveform with an apparent DC offset, which appears as power at 0 Hz in the power spectrum. A second aliased peak at roughly 4 Hz can also be seen in the spectrum for the 10-Hz sampling rate.

In conventional digital EEG practice, aliasing error is avoided by applying an analog low-pass filter that eliminates the power at frequencies greater than the Nyquist frequency. To sample the time series of Figure 1 at 20 Hz, both the 10 and 19 Hz must be removed in the analog signal prior to digitization. Similarly, to digitally sample EEG at rates below 150 samples per second, analog filters are used to remove the power at the 60-Hz (or 50-Hz) line (or mains) frequency in order to prevent aliasing of this noise into the lower frequency bands that make up the EEG.

The Nyquist criterion for discrete sampling applies to spatial as well as to temporal sampling of EEG. The scalp surface potential at any point in time is a continuous field over the surface of the head. The sensor (electrode) array effects a discrete sampling of this field, and this sampling is subject to the Nyquist criterion. Unlike the time series of a single amplifier channel, the spatial signal is acquired discretely. The temporal signal can be low-pass filtered to remove aliasing information prior to digitization, but the spatial signal cannot. As a consequence, any aliasing on account of undersampling cannot be undone, and it is critical that an adequate sampling of the potentials be accomplished from the outset. The electrode density (assuming an evenly distributed electrode placement) determines the highest spatial frequency that can be observed without aliasing.

A local estimate of the sampling density required for human EEG and ERP measurements was obtained by Spitzer, Cohen, Fabrikant, and Hallett (1989). These investigators placed coronal and sagittal rows of closely spaced electrodes on the scalp and then measured the sub-

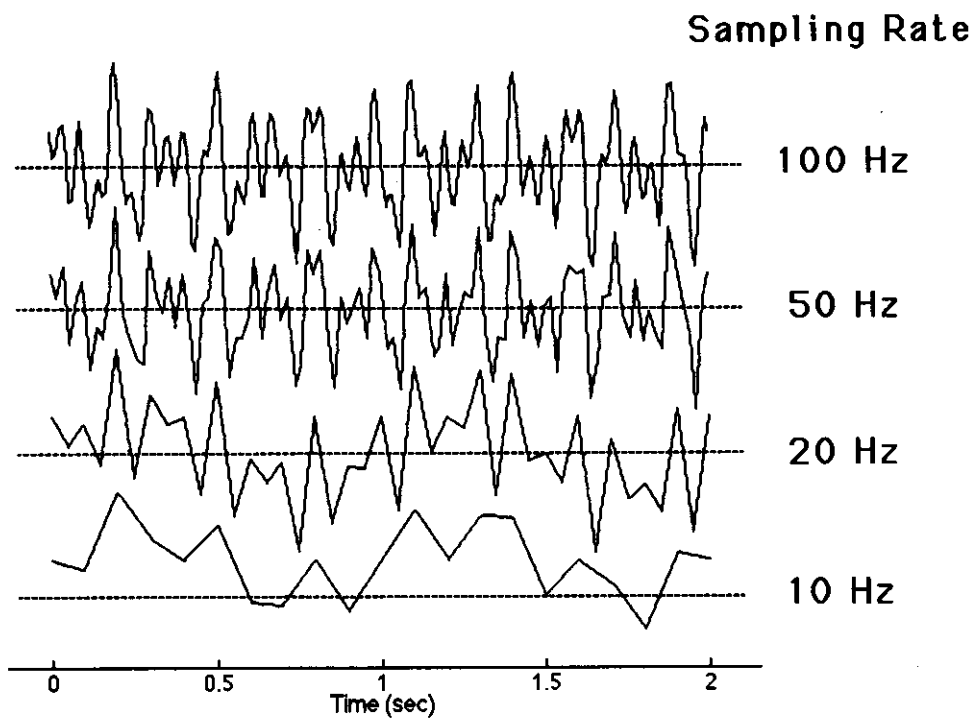

Figure 1A. Composite signal (6.5-, 10-, and 19-Hz sine waves) sampled above (50 and 100 Hz) and below (20 and 10 Hz) the Nyquist frequency.

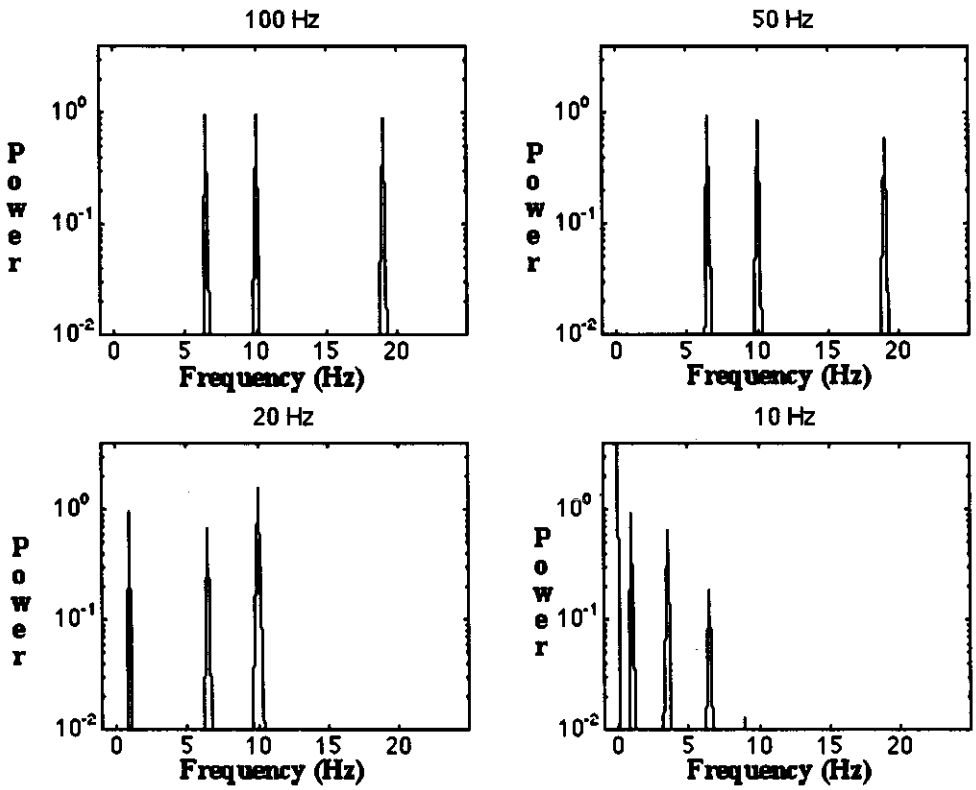

Figure 1B. Power spectral analysis of the adequate (100 Hz and 50 Hz) and inadequate (20 Hz and 10 Hz) digital sampling of the composite signal in Figure 1A. Inadequate discretization results in temporal aliasing, in which frequencies present in the time series are not characterized and are instead misrepresented as lower frequencies.

ject's somatosensory ERP. Spitzer et al. concluded that a sensor spacing of less than 3 cm is required, in contrast with the typical 7-cm intersensor distance obtained with the International Ten–Twenty System locations. For an even (geodesic) sampling of the head surface, the intersensor distance decreases linearly as the sensor count doubles. For a 32-sensor array, the intersensor distance for an average adult head is somewhat less than 5 cm; for a 64-sensor array, it is slightly less than 4 cm; and for a 128-sensor array, it is slightly less than 3 cm (Tucker, 1993).

To obtain global estimates of the Nyquist limit implied by spatial sampling in EEG, we approximate the head by a sphere whose two spatial dimensions are represented by the azimuth (f, $0 < f < 360$) and elevation (q, $0 < q < 180$). The azimuth is the angle describing the position on the plane at the equator of the sphere (longitude), and the elevation describes the position from north to south pole (latitude). Together, these spherical coordinates can address all points on the sphere surface. Spatial frequencies on the sphere are defined in terms of the orthogonal basis functions for spherical surfaces, the spherical harmonics $Y_{nm}(q,f)$. These are analogous to the sine and cosine basis functions that are used in the Fourier decomposition of the time series in EEG spectral analysis. Just as any time series of EEG signal can be described by its power spectrum (coefficients applied to each of the series of sine waves), any potential field that is defined on a sphere can be represented as a weighted sum of spherical harmonics. In neither temporal nor spatial freqencies is the analysis limited to sine waves; the decomposition describes the frequency spectrum of the actual data series in time or space. An example is the spherical harmonic decomposition of the potential field that is due to a dipole current source in the brain (Nunez, 1981; Srinivasan, Nunez, & Silberstein, in press).

Any spherical harmonic of degree n is related to other spherical harmonics of the same degree by rotating the coordinate system, so that unique spatial frequencies are determined by the degree n (McLeod, 1980; McLeod & Coleman, 1980). Correspondence to wavenumbers k (1/cm) is obtained as $k = (n + 1)/R$, where R is the radius of the sphere (typically ~9 cm). Examples of spherical harmonics of degrees 4 and 7 are shown in Figure 2. The top row shows the spherical harmonic of degree 4 for both the azimuth and elevation of the spherical coordinates. The bottom row shows the same azimuth frequency (four cycles across the circumference) but with an elevation harmonic of degree 7.

The 128-channel Geodesic Sensor Net is a device for distributing EEG sensors in an even pattern across the head surface (Tucker, 1993). It spans an elevation of 120° (measured from vertex toward the neck). Because it cov-

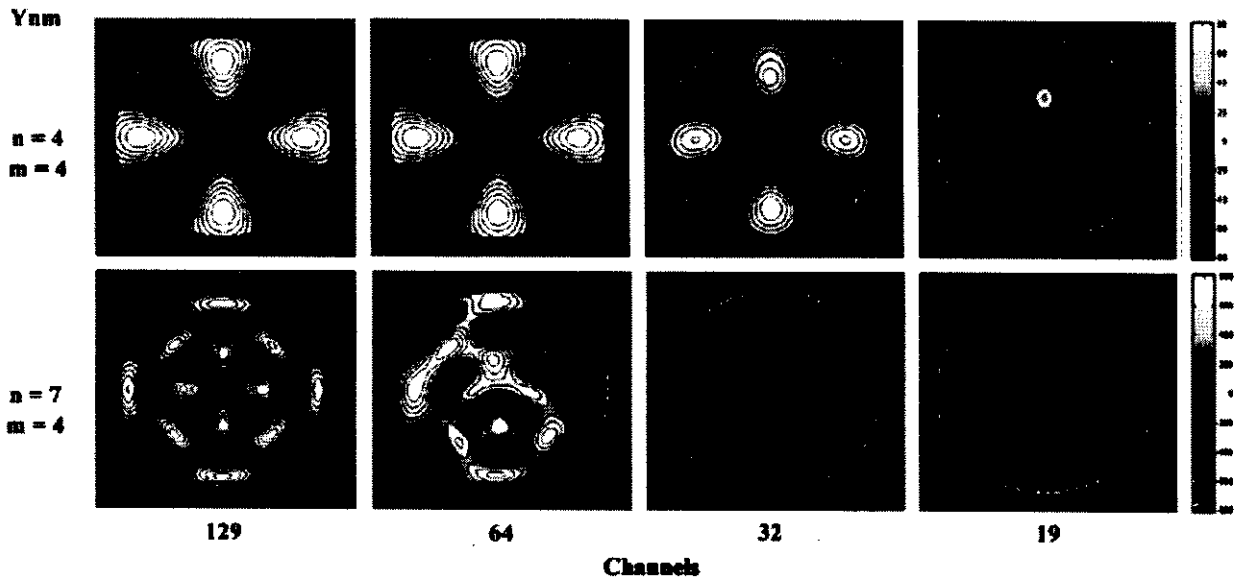

Figure 2. Sampling of two examples of spatial frequency with 129-, 64-, 32-, and 19-channel sensor arrays. In all of the 2-D topographic (circle) plots, the view is looking down on the top of the head, with the nose at the top. The top row shows four cycles of azimuth and four cycles of elevation. Acceptable accuracy is shown for the 32-channel array, but not for the 19-channel array. The bottom row shows four cycles of azimuth and seven of elevation. Only the 129-channel array provides accurate sampling.

ers the majority of the head surface, the average potential across all channels begins to approximate the surface integral of the scalp potential field. Because all sources are dipolar, the sum of all positive and negative fields (the surface integral) must be zero. When the average reference is computed under these conditions, it can be assumed to differ from the zero potential of the head by the potential at the reference sensor (in this case the vertex), producing an additional data channel (129). We have observed that, with 16 and 32 channels, this assumption is inaccurate. The average potential of the set of channels typically varies from zero by a larger quantity that seems reasonably attributable to the reference site, indicating that there are large surface potentials that have not been sampled. With 64-channel sampling that extends inferiorly to the canthomeatal line, the average reference was found to be small, and the waveform appeared appropriate for the recording reference (right mastoid) site (Curran, Tucker, Kutas, & Posner, 1993).

Spherical harmonics up to degree $n = 7$ can be sampled with this array of electrodes without aliasing (i.e., seven cycles across the surface). However, we found that spherical harmonics of degree $n = 9$ are visibly distorted. With 64, 32, and 19 electrodes corresponding to the International Ten–Twenty System, the highest spherical harmonics that can be sampled without aliasing are $n =$ 6, 4, and 3, respectively. Figure 2 shows the spherical harmonics $Y_{44}(q,f)$ and $Y_{74}(q,f)$ sampled with each of these arrays. Both spherical harmonics are accurately sampled by the 129-channel array. As the number of sensors is reduced to 64, the Y_{74} spatial frequency aliases, whereas at 19 channels the Y_{44} frequency aliases.

To put this analysis in perspective, assume a 9 cm radius for the average head (54.5 cm circumference); the Y_{44} period would be 14.1 cm. The smallest topographic feature that can be resolved accurately by a 32-channel array is therefore 7 cm in diameter (a half-cycle of the Y_{44} period), or about the size of a lobe of the brain. Remarkably, an electrical field of this size is seriously aliased by the 19-channel recording of the clinical EEG. This example illustrates how undersampling the higher spatial frequencies of the EEG not only fails to characterize the topographic detail; the high frequency information aliases into lower spatial frequencies, thus distorting the apparent scalp topography of the electrical field.

The properties of this aliasing can be quantified in the same way as with a time series analysis—by examining the power spectrum over spatial frequencies (Srinivasan, 1995; Srinivasan, Nunez, Tucker, Silberstein, & Cadusch, 1996). Figure 3 shows the power spectrum over spherical harmonic degree for a signal consisting of the spherical harmonic of degree 7 as it would be recorded with each of the sensor arrays discussed here. Only the 129-channel array accurately assesses the power spectrum of this spherical harmonic. Each of the other arrays aliases the power to lower spatial frequencies.

SPATIAL LOW-PASS FILTERING BY THE HEAD

From the example of time series in Figure 1 and that of spherical harmonics in Figure 2, it is evident that the required sampling rate is determined by the highest frequency present in the signal, whether the sampling is spatial (electrode density) or temporal (analog-to-digital conversion rate). Whereas, for temporal sampling, antialiasing filters can be applied according to the Nyquist criterion (e.g., low-pass filtering at 40 Hz to allow sam-

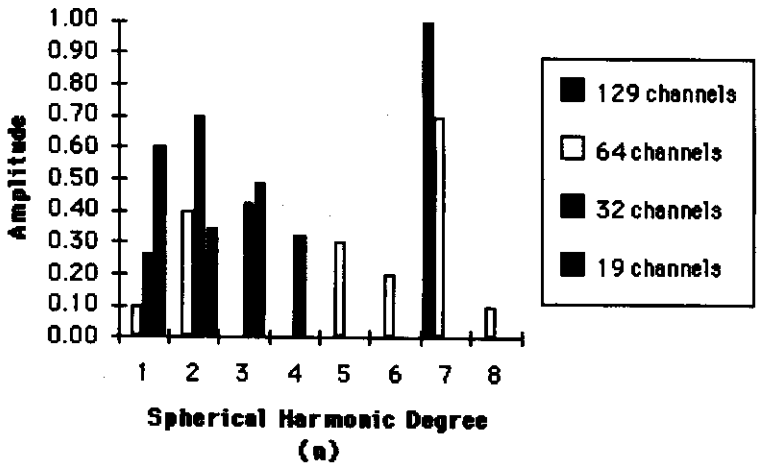

Figure 3. Spatial frequency spectrum (in the elevation dimension) for the spherical harmonic of degree 7 with 129-, 64-, 32-, and 19-channel arrays. Only the 129-channel array characterizes this frequency accurately.

pling at 100 Hz), this is not possible for the inherently discrete sampling of individual scalp sensors. However, nature has conveniently provided us with an anti-aliasing spatial filter in the form of the poorly conducting skull. It is evident that the smearing of the cortical potentials by the poorly conducting skull limits the spatial resolution of scalp EEG (Nunez, 1981; Srinivasan et al., 1996), but it actually makes the discrete sampling problem a manageable one. The effect of the poorly conducting skull is to low-pass spatial filter the scalp potentials, and this can be modeled by a four-concentric-spheres (brain, cerebrospinal fluid, skull, and scalp) simulation of the head. In this model, the relationship between a dipole source and the scalp surface potentials can be written as a series of spherical harmonics for both radial and tangential dipoles (see Srinivasan et al., in press, for details).

In general, we can expect a distribution of sources throughout the brain. At any fixed depth, this distribution can itself be written as a sum over spherical harmonics. We have shown that the spatial frequency components of the source distribution are differentially filtered by the skull, which attenuates the high spatial frequencies of cortical source activity (Srinivasan et al., in press; Srinivasan et al., 1996). This transfer function is plotted in the case of a superficial dipole layer in Figure 4A. The simulations that follow are limited to this case, because superficial sources contribute most to the EEG at high spatial frequencies because of the proximity of sources and electrodes. The transfer function shows the relative magnitudes of the contributions of spherical harmonic components of cortical source distributions to scalp potentials. This figure suggests that we can expect that scalp potentials increasingly attenuate as source spatial frequency increases, making it possible to achieve a sampling of scalp potentials with minimal aliasing with a reasonable number of electrodes.

Figure 2 illustrated that the electrode density determines the highest spatial frequency observed by the array. We used each of the sensor arrays to sample the scalp potential field with a power spectrum that falls off with high spatial frequencies (modeling that of the head), as shown in Figure 4A. The potential field that is due to a single dipole source has this spatial power spectrum. This is also equivalent to assuming that the underlying cortical source distribution is spatial white noise (i.e., having equal power at all spatial frequencies; Srinivasan et al., 1996). Figure 4B shows estimates of the spatial power spectrum obtained with each electrode array. By contrast to the true spectrum shown in Figure 4A, each of the arrays shows somewhat higher power at lower spatial frequencies. This increase is due to signals at higher spatial frequencies aliasing into lower spatial frequencies. The fall-off of amplitude with spatial frequency is also somewhat distorted. In the case of a small number of electrodes (19 or 32), the aliased signal is pronounced over the wavenumbers $n = 2$ to $n = 4$. The 64-channel sampling appears adequate for wavenumbers up to 5. In the case of 129 channels (128 plus the regenerated reference), the aliasing is limited, with slightly higher amplitude at lower spatial frequencies and a fall-off function that is similar to the theoretical transfer function.

In this simplified head model, the 129-channel array appears to approach an adequate sampling of scalp potentials. However, our model does not include important features of real heads (e.g., eye sockets, thinner temporal bone, etc.) that may influence the sampling problem. Furthermore, our simulations were based on the assumption that cortical amplitude at least remains constant (but likely decreases) with increasing spatial frequency (Nunez, 1981; Pfurtscheller & Cooper, 1975; van Rotterdam, Lopes da Silva, van den Ende, Viergever, & Hermans, 1982). Furthermore, the key factor for simulation and source localization studies is the conductivity of the skull, which, although widely assumed to be 80 times the conductivity of the brain, is in fact unknown (Law, 1993).

There are thus important differences between the human EEG and the spherical model of these simulations. Obtaining converging evidence on the simulations is im-

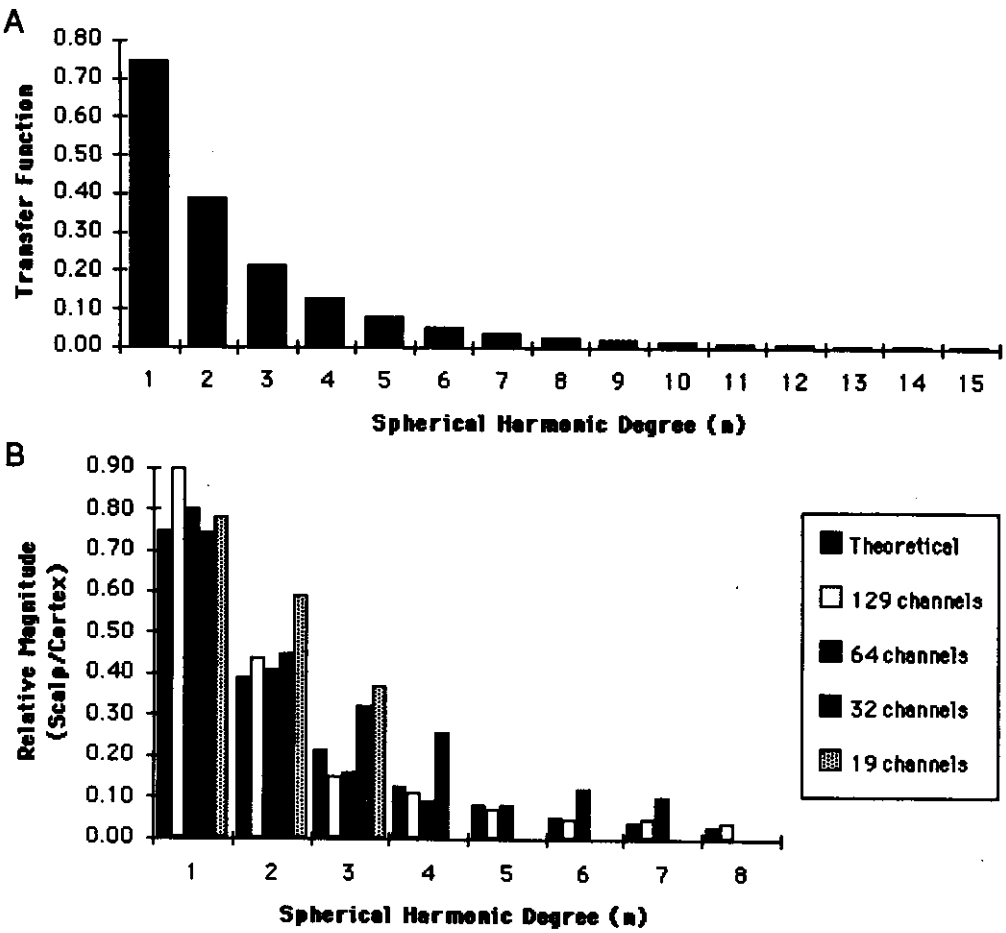

Figure 4. (A) Theoretical transfer function of brain electrical sources through the skull. The high spatial frequency components are attenuated by the poorly conducting skull. (B) Transfer function as sampled with 129, 64, 32, and 19 channels. The inflation of lower spatial frequencies is due to spatial aliasing.

portant, because, if they are correct, they demonstrate that conventional EEG electrode arrays (19–32) are inadequate, and a 64-channel array is marginal at best. The fundamental question for modeling the adequate sampling density is the spatial frequency content of the scalp EEG that is passed through the skull. In the next section, we examine a sample of human EEG in order to assess its spatial frequency with a 128-channel array and to determine the effects of subsampling this array with conventional EEG channel counts.

SPATIAL SAMPLING OF THE HUMAN VISUAL ERP

A sample of a visual ERP was selected from a normal adult subject (D.M.T.). The peak of the N1 component (200 msec) was chosen as a well-known feature with a distinct scalp topography. Two examples of averaged ERP data were examined from a simple target-detection (visual oddball) paradigm, with 80% standards (the letter *O* presented at fixation) and 20% targets (*X*). The target ERP was examined in each case. The subject responded as quickly as possible to targets and did not respond to standards. The first example is from a typical run of 250 trials (50 targets), with 43 artifact-free epochs of EEG included in the average. The second ERP example is from an atypical ERP run, conducted while testing the experimental setup, including only 100 trials (20 targets), with 12 artifact-free epochs in the average. This ERP showed a much larger P300, which is consistent with the subject's report that the first few trials of the task engage normal attention, whereas, after many repetitions, the task induces perceptual habituation, attentional fatigue, and the subjective experience of mental numbing.

Interestingly, the N1 to the short run of trials showed a topographic feature that is consistent with the subjective report of intact attention: a temporal lobe extension of the N1 distribution. Potts, Liotti, Tucker, and Posner (1996) examined a visual oddball paradigm, with the digits 2 or 4 presented at fixation in 80%–20% proportions and with instructions to count the targets for attended blocks and to simply watch the stream of digits for unattended blocks. On attended blocks, the later topography of the N1 (after the initial bilateral foci)

showed an extension of the negativity toward the temporal lobes. For the present purposes, the increased temporal lobe negativity of the short run of trials created scalp topographic detail that can be examined in terms of the required sampling density for adequate measurement.

The data were recorded with the 128-channel Geodesic Sensor Net (Tucker, 1993), with a vertex recording reference. Initial interpolated maps were created with the 129-channel data, using the average reference. For interpolation, both spherical spline and linear methods were used, with generally similar results. The spherical splines method (Perrin, Pernier, Bertrand, & Echallier, 1989) adjusts the coefficients of the spherical harmonics to fit a continuous surface to the measured locations. This method produced smoother contours than did the linear nearest-neighbor interpolation and was used for all of the data reported here.

To estimate the loss of spatial detail and the possibility of spatial aliasing caused by inadequate sampling density, a subsampling of the 128 sensors to 64 sensors was performed by selecting the even-numbered channels. As a contrast, a second 64-channel subsampling was performed with the odd-numbered channels. Spherical spline interpolated maps were created to estimate the quality of the prediction of the 128-channel topography from the 64-channel subsamplings. A 32-channel subsampling was performed as a regular geodesic subset of the 128-channel layout. To improve the anchoring of the 32-channel montage about the eyes and face (where large gradients are often seen), infraorbital and external canthus channels were included within the 32. Finally, the sensors at the locations of the conventional 19 channels of the International Ten–Twenty System were also used to interpolate the potential surface. The sensors represent-

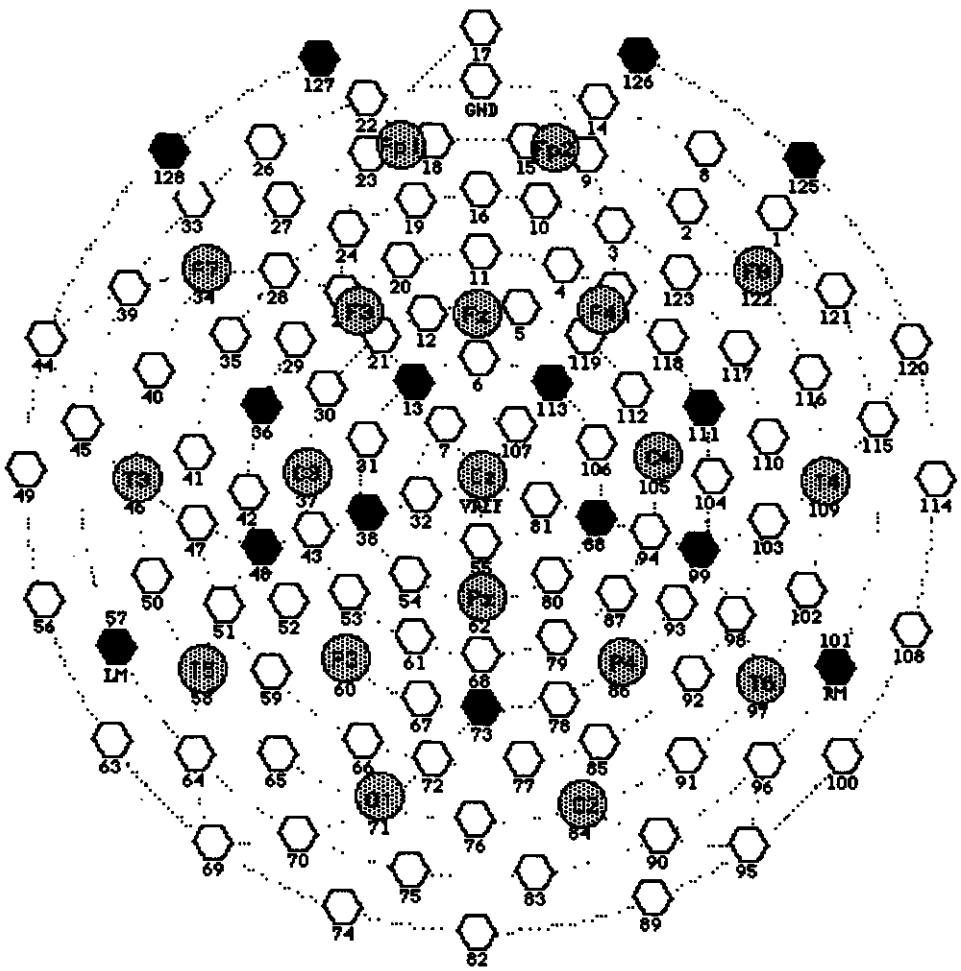

Figure 5. Sensor Layout of 128-channel Geodesic Sensor Net and approximate International Ten–Twenty System locations. The alternate 64-channel arrays comprised odd- and even-numbered channels. In addition to the Ten–Twenty locations, the 32-channel montage included the channels marked by gray hexagons.

ing F3, F4, and Fp1, Fp2 of the International Ten–Twenty System are approximately 0.5 to 1 cm more lateral in the Geodesic Sensor Net than are the actual measured locations of the Ten–Twenty System. Of course, because they were not explicitly measured, all of the Ten–Twenty locations are only approximations. Figure 5 shows the layout of the Geodesic Sensor Net with the approximate Ten–Twenty locations and the additional sensors used for the 32-channel subset.

Visual N1 From the Long Run

Figure 6 shows the N1 to the targets for the 43-trial average, appearing as two bilateral negative foci at about 180 msec, coincident with a right-lateralized anterior positivity (the P2). The images in Figures 6–12 were scaled with the same palette, shown at the right of the figures, with positive indicated by the light end of the palette and negative indicated by the dark end of the palette. Figure 6A shows the data in a two-dimensional polar projection (looking down on the head, left side on the left, nose at the top). Because the Geodesic Sensor Net extends more inferiorly than do other electrode methods, it is important to orient the polar map with the sensor positions on the three-dimensional (3-D) head. Figure 6B is a schematic of a 3-D head that shows the realistic surface distribution of this N1 map.

The 128-channel Geodesic Sensor Net has a geodesic frequency of four, meaning that there are four divisions of each leg of the major triangles of the icosahedron (and 16 minor triangles within each major face of the icosahedron). This montage cannot be subsampled to 64 sensors with a regular geodesic pattern. The 64-channel geodesic would require a geodesic frequency of three, producing vertices that do not overlap with those of the 128-channel pattern. Therefore, a 64-channel subsampling was achieved by selecting the even channels of the 128-channel array. The channel numbers are aligned in radial rows, from the outer ring toward the vertex (Figure 5), such that the selection of even-numbered channels results in a fairly regular subsampling of the 128-sensor set.

Figure 7A shows the data from Figure 6, now subsampled with the even 64 channels. The representation of the general topography is good, with only a moderate loss of local detail. Figure 7B shows the same data subsampled with the odd 64 channels. The general form of the field patterns is retained, with bilateral posterior negative foci and a frontal positivity. However, not only is there a loss of detail, but the spatial aliasing causes the general topography to be distorted fairly severely. The odd and even 64-channel subsets are fairly well balanced in location, but they are not as evenly distributed as a geodesic array. It is clear that, in this particular voltage topography, these montages yield substantially different samplings of the scalp field.

More severe subsampling of the 128-channel recording was carried out with 32- and 19-channel montages. The 32-channel subsampling, Figure 8A, followed the geodesic pattern. Examining the gray hexagons and the Ten–Twenty locations in Figure 5, this pattern included channels 9, 11, 13, 23, 25, 34, 36, 38, 46, 48, 57, 58, 60, 62, 71, 73, 84, 86, 88, 97, 99, 101, 111, 113, 122, 124, 125, 126, 127, 128, and 129 (the recording reference at Cz). The 19-channel subsampling, Figure 8B, used the sensors approximating the International Ten–Twenty locations, including channels 9, 11, 23, 25, 34, 37, 46, 58, 60, 62, 71, 84, 86, 97, 105, 109, 122, 124, and 129.

For both the 32- and 19-channel montages, the N1/P2 topography shows the broad outline of an anterior positivity and a posterior, more focal negativity. However, the degradation of the actual field topography was severe in both cases. For the N1 focus itself, small left–right asymmetries of the original scalp field topography (Figure 6A) resulted in large asymmetries in the sparse array interpolations, because of the accidental relations between the few sensor locations in the region of the N1 and the actual gradients of the N1 focus. Thus, the region of the left hemisphere N1 was not sampled by the T5

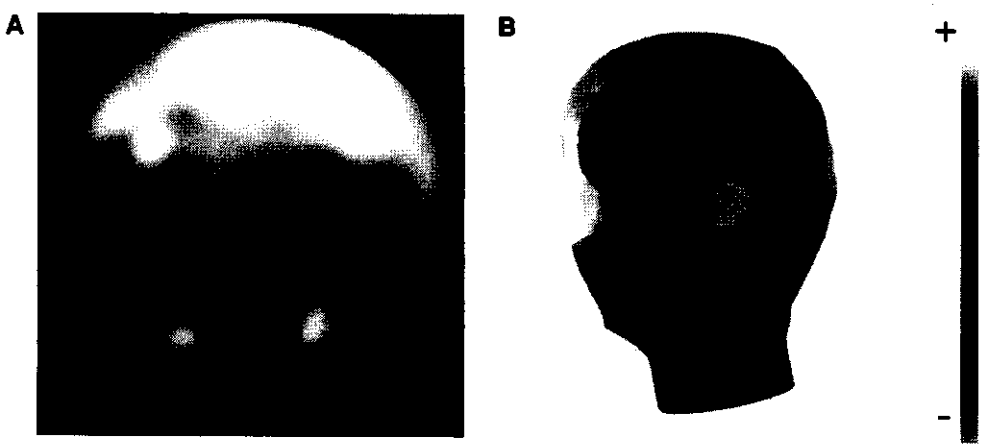

Figure 6. N1 of the visual ERP recorded with 128 channels. (A) 2-D polar projection. (B) 3-D schematic on a realistic head shape.

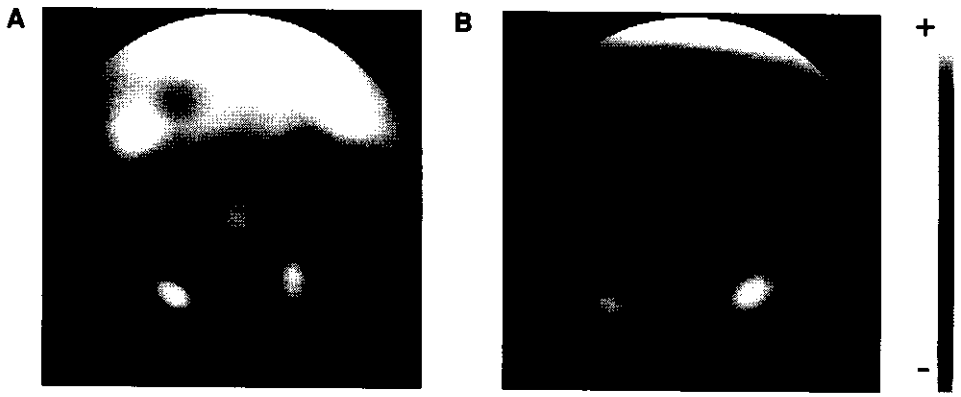

Figure 7. The data from Figure 6 subsampled with (A) the 64 even sensors and (B) the 64 odd sensors.

(channel 71) site, whereas the right hemisphere N1 was sampled by the T6 (channel 97) site. Although the asymmetry of this subject's N1 is in reality fairly subtle, it becomes distorted by the inadequate spatial sampling of 32- and 19-channel montages and by inappropriate interpolation from the poorly measured voltage surface.

Visual N1 From the Short Run

The more detailed N1 seen in the short run of trials (12 artifact-free epochs) is shown in Figure 9. The distribution of these fields on a 3-D head shape is shown in Figure 10. Some of the high spatial frequency of this image is almost certainly due to the small number of trials in the average. However, it seems unlikely that the distinct temporal lobe progression of this N1 is due to sampling noise, particularly given the previous observation of this effect in response to attentional manipulation (Potts et al., 1996). It can be seen simply from visual inspection of Figure 9 that the negative fields of the N1 are quite focal—as focal as could be measured by the 128-channel density of this recording. Without oversampling (i.e., a 256-channel recording), it is not possible to determine whether there were higher spatial frequency components of this electrical event that were undersampled by the 128-channel array.

However, it is possible to subsample this map and examine the adequacy of lower channel counts. Figure 11A shows the sampling with the even-numbered, and Figure 11B shows it with the odd-numbered 64-channel subsets. Although the N1 was detected on both sides of the image, neither its topography nor that of the centrofrontal positivity was characterized accurately. Figures 12A and 12B show the 32- and 19-channel subsamplings, respectively. Neither is acceptable. The contrast between the information in Figure 9 and that in 12b shows the inadequacy of measurement of the Ten–Twenty System.

CONCLUSIONS AND RECOMMENDATIONS

Both the theoretical simulations and the subsampling of a sample of the visual ERP showed similar results. Adequate spatial sampling of the brain's electrical field at the scalp surface requires a sufficient density of potential measurements. If the sensors are distributed across the full surface of the head, a minimum of 128 channels appears necessary in order to characterize the full range

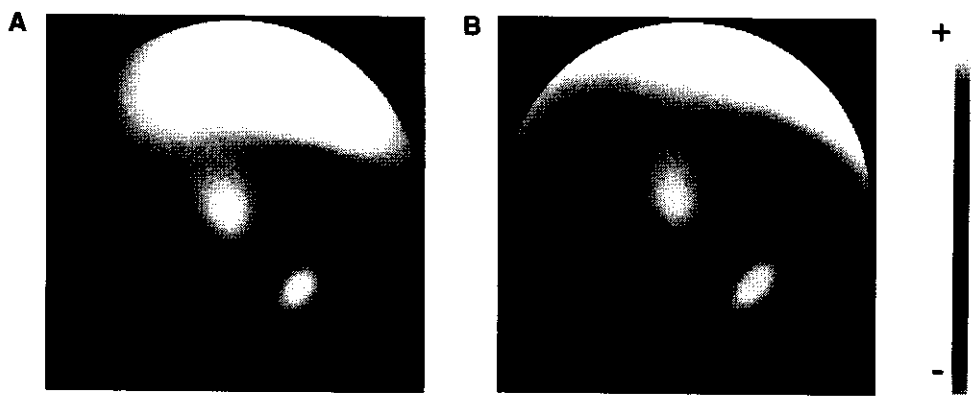

Figure 8. Data from Figure 6 subsampled further. Figure 8A shows a 32-channel sample in the geodesic pattern of the 128-channel Net. Figure 8B shows the data sampled with the 19 channels approximating the International Ten–Twenty System.

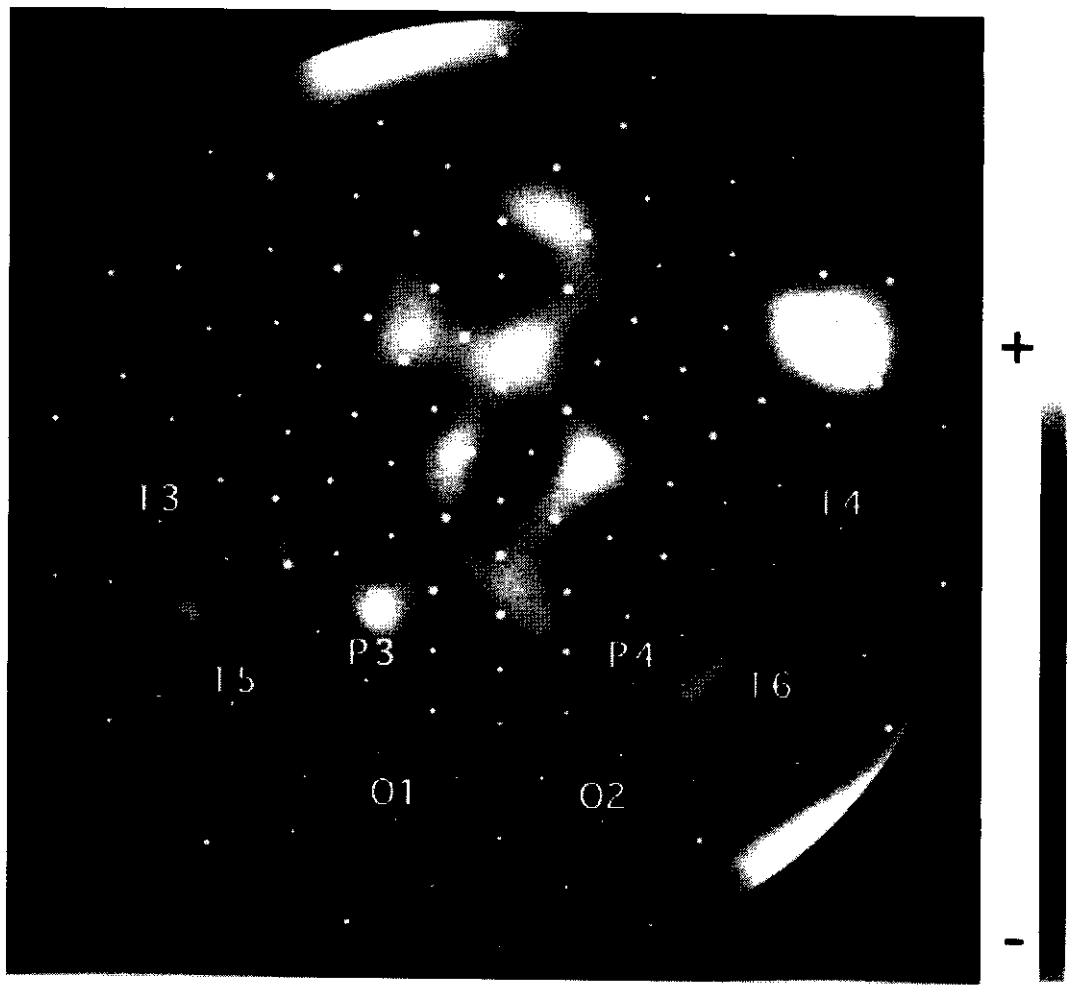

Figure 9. Visual N1 of the same subject, measured with 128 channels, averaged over the initial 12 targets. The Ten–Twenty label is placed directly above (anterior to) the sensor location. Some sensor marks blended with the image color and are not visible.

of spatial detail in the brain's electrical fields at the scalp surface.

In each example, there was both undersampling of the topographic pattern and aliasing of high spatial frequencies into lower spatial frequencies in the 32- and 19-channel maps. The effect of spatial aliasing was to make the interpolated maps appear to be smooth when, in fact, the actual dense array measurements showed that the scalp electrical field was not. Furthermore, in certain cases, there was significant spatial aliasing with 64 channels, such that focal electrical fields or sharp field gradients were not adequately characterized. The critical issue for adequate spatial sampling is, of course, not the total number of channels, but intersensor distance. A 32-channel montage could be concentrated on a single area, such as over the motor strip, with 1-cm intersensor distances to achieve oversampling of the spatial topography (Spitzer et al., 1989).

For laboratories sampling the full head surface with 32 and fewer channels, visualization and data analysis should proceed with waveform plots rather than with maps, because interpolated maps convey the misleading impression of a smooth potential surface. Furthermore, the average reference is not adequately estimated with a sparse sensor array, particularly given the poor sampling of the inferior head surface with the Ten–Twenty montage. Therefore, the data from a sparse montage must remain in referenced waveforms. However, accurate and informative descriptions can be gained from waveforms from a sparse montage (32 and fewer channels). In presenting referenced waveforms (e.g., with a mastoid, ear, or nose reference electrode), the reference cannot be assumed to remain at zero potential (Nunez, 1981). Rather than the typical practice of labeling the waveform as if it were recorded from *one* of the sensors that make up the amplifier channel (e.g., "F3"), the waveform from a channel of a differential amplifier should be labeled as the bipolar sensor pair it represents (e.g., "F3-A1"). By understanding that each recording channel is inherently bipolar, ERP researchers with sparse sensor arrays can

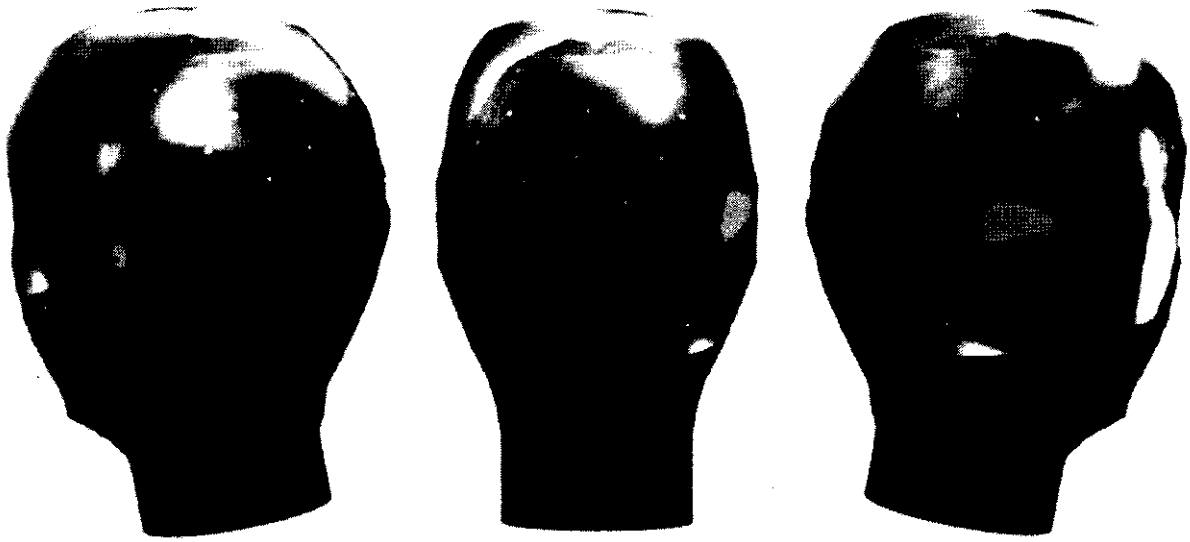

Figure 10. Distribution of the data from Figure 9 on a realistic head shape.

interpret their bipolar pairs accurately, as clinical electroencephalographers have done for a half century (Walter, 1950).

The present data are, of course, preliminary. Further studies are required in order to determine the spatial frequency of each of the phenomena of the ERP and EEG that are of clinical or research interest. With 128-channel recordings now being made in many laboratories, there does not appear to be a clear asymptote in the scalp topography when the 128-channel data are compared with 64-channel recordings. Instead, there are many examples in which the 128-channel maps show a striking increase in topographic detail. Without an asymptote in information yield, it is not possible to characterize the spatial Nyquist of the human EEG with confidence. Even if 128-channel sampling is adequate, empirical studies with 256-channel recordings will be necessary to determine that oversampling—that is, no increment in spatial frequency—has been achieved. Advanced electrical analysis methods, such as computing skull current density with Laplacian measures or attempting source localization with inverse solutions, place even greater demands on spatial sampling than does the analysis of potential data (Srinivasan et al., 1996). These methods will be particularly misleading with low sensor densities.

It is clear that progress in understanding the spatial information in the human EEG will require research with dense sensor arrays. Advances in amplifier electronics, computer software, and scalp sensor arrays have allowed dense array EEG systems to be developed, commercially or in university laboratories, for a fraction of the cost of other neuroimaging methodologies such as MEG, fMRI, or PET (Tucker, 1993; Virtanen, Rinne, Ilmoniemi, & Näätänen, 1996; Wikswo, Gevins, & Williamson, 1993). The temporal resolution of EEG is identical to that of MEG, and both are superior to hemodynamic measures by two orders of magnitude (milliseconds vs. seconds). Whether MEG confers advantages in spatial resolution over the EEG is now a matter of debate (Cohen et al., 1990; Malmivuo, Suihko, & Eskola, 1997; Wikswo et al., 1993).

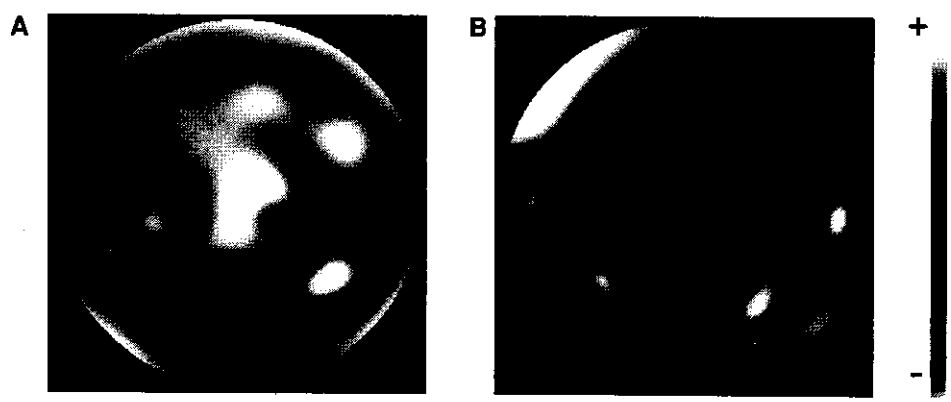

Figure 11. The data of Figure 9 subsampled with the 64 even (A) and 64 odd (B) sensors.

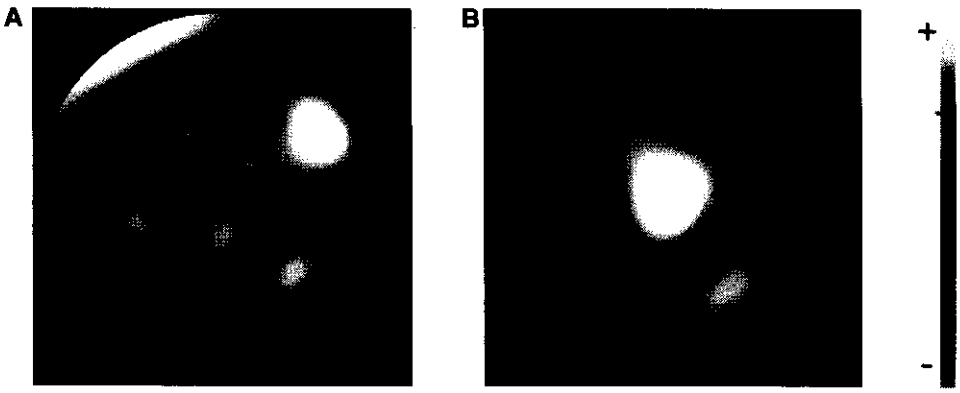

Figure 12. The data of Figure 9 subsampled with 32 channels (A) and with the 19 channels approximating the International Ten–Twenty System (B).

Coupled with advances in electrical source localization, dense sensor array EEG may be the most cost-effective approach to neuroimaging now available, adding critical anatomical context to the rich temporal information of scalp electrical recordings.

REFERENCES

BENDAT, J. S., & PIERSOL, A. (1986). *Random data: Analysis and measurement procedures*. New York: Wiley.

COHEN, D., CUFFIN, B. N., HUNOKUCHI, K., MANIEWSKI, R., PURCELL, C., COSGROVE, G. R., IVES, J., KENNEDY, J. G., & SCHOMER, D. L. (1990). MEG versus EEG localization test using implanted sources in the human brain. *Annals of Neurology*, **28**, 811-817.

CURRAN, T., TUCKER, D. M., KUTAS, M., & POSNER, M. I. (1993). Topography of the N400: Brain electrical activity reflecting semantic expectation. *Electroencephalography & Clinical Neurophysiology*, **88**, 188-209.

LAW, S. K. (1993). Thickness and resistivity variations over the upper surface of the human skull. *Brain Topography*, **6**, 99-109.

MALMIVUO, J., SUIHKO, V., & ESKOLA, H. (1997). Sensitivity distributions of EEG and MEG measurements. *IEEE Transactions on Biomedical Engineering*, **44**, 196-208.

MCLEOD, M. G. (1980). Orthogonality of spherical harmonic coefficients. *Physics of the Earth & Planetary Interiors*, **23**, P1-P4.

MCLEOD, M. G., & COLEMAN, P. J. (1980). Spatial power spectra of the crustal geomagnetic field. *Physics of the Earth & Planetary Interiors*, **23**, P5-P19.

NUNEZ, P. L. (1981). *Electric fields of the brain: The neurophysics of EEG*. New York: Oxford University Press.

PERRIN, F., PERNIER, J., BERTRAND, D., & ECHALLIER, J. F. (1989). Spherical splines for scalp potential and current density mapping. *Electroencephology & Clinical Neurophysiology*, **72**, 184-187.

PFURTSCHELLER, G., & COOPER, R. (1975). Frequency dependence of the transmission of EEG from cortex to scalp. *Electroencephalography & Clinical Neurophysiology*, **42**, 817-826.

POTTS, G. F., LIOTTI, M., TUCKER, D. M., & POSNER, M. I. (1996). Frontal and inferior temporal cortical activity in visual target detection: Evidence from high spatially sampled event-related potentials. *Brain Topography*, **9**, 3-14.

SPITZER, A. R., COHEN, L. G., FABRIKANT, J., & HALLETT, M. (1989). A method for determining optimal interelectrode spacing for cerebral topographic mapping. *Electroencephalography & Clinical Neurophysiology*, **72**, 355-361.

SRINIVASAN, R. (1995). *A theoretical and experimental study of neocortical dynamics*. Unpublished doctoral dissertation, Tulane University, New Orleans.

SRINIVASAN, R., NUNEZ, P. L., & SILBERSTEIN, R. B. (in press). Spatial filtering and neocortical dynamics: Estimates of EEG coherence. *IEEE Transactions on Biomedical Engineering*.

SRINIVASAN, R., NUNEZ, P. L., TUCKER, D. M., SILBERSTEIN, R. B., & CADUSCH, P. J. (1996). Spatial sampling and filtering of EEG with spline Laplacians to estimate cortical potential. *Brain Topography*, **8**, 355-366.

TUCKER, D. M. (1993). Spatial sampling of head electrical fields: The geodesic sensor net. *Electroencephalography & Clinical Neurophysiology*, **87**, 154-163.

VAN ROTTERDAM, A., LOPES DA SILVA, F. H., VAN DEN ENDE, J., VIERGEVER, M. A., & HERMANS, A. J. (1982). A model of the spatial-temporal characteristics of the alpha rhythm. *Bulletin of Mathematical Biology*, **44**, 283-305.

VIRTANEN, J., RINNE, T., ILMONIEMI, R. J., & NÄÄTÄNEN, R. (1996). MEG-compatible multichannel EEG electrode array. *Electroencephalography & Clinical Neurophysiology*, **99**, 568-570.

WALTER, W. G. (1950). Normal rhythms—Their development, distribution, and significance. In D. Hill & G. Parr (Eds.), *Electroencephalography* (pp. 203-227). London: McDonald.

WIKSWO, J., GEVINS, A., & WILLIAMSON, S. (1993). The future of MEG and EEG. *Electroencephalography & Clinical Neurophysiology*, **87**, 1-9.